Kent Academic Repository

Versions of research works

Versions of Record
If this version is the version of record, it is the same as the published version available on the publisher's web site. Cite as the published version.

Author Accepted Manuscripts
If this document is identified as the Author Accepted Manuscript it is the version after peer review but before type setting, copy editing or publisher branding. Cite as Surname, Initial. (Year) 'Title of article'. To be published in *Title of Journal* , Volume and issue numbers [peer-reviewed accepted version]. Available at: DOI or URL (Accessed: date).

Enquiries
If you have questions about this document contact ResearchSupport@kent.ac.uk. Please include the URL of the record in KAR. If you believe that your, or a third party's rights have been compromised through this document please see our Take Down policy (available from https://www.kent.ac.uk/guides/kar-the-kent-academic-repository#policies).

IET Control Theory & Applications

The Institution of Engineering and Technology   WILEY

ORIGINAL RESEARCH PAPER

Hierarchical global fast terminal sliding-mode control for a bridge travelling crane system

Weilin Yang[1] | **Jiayu Chen[1]** | **Dezhi Xu[1]** | **Xinggang Yan[2]**

[1] School of Internet of Things Engineering, Jiangnan University, Wuxi, China

[2] School of Engineering and Digital Arts, University of Kent, Canterbury, UK

Correspondence
Dezhi Xu, School of Internet of Things Engineering, Jiangnan University, Wuxi, 214122, China.
Email: lutxdz@126.com; xudezhi@jiangnan.edu.cn

Abstract

The bridge crane system is a typical under-actuated system that is widely used in production and life. Although various scholars have conducted extensive research on the bridge crane system in recent years, there are still many problems, such as the trajectory planning of the cart and the anti-sway control of the cargo. In order to tackle the problem of the anti-sway control of the cargo, a hierarchical global fast terminal sliding-mode control (H-GFTSMC) is developed in this work. First, the Lagrange equations are used to model the system dynamics. Then, an appropriate hierarchical global fast terminal sliding-mode controller is designed to achieve anti-sway control of the cargo, and it is proved that each sliding-mode surface is progressively stable. A series of simulations were implemented to verify the effectiveness of the control method. The simulation results show that the H-GFTSMC has better control performance compared with the proportional–integral–derivative control method. When changing the cable length or adding non-negligible noise to the system, the H-GFTSMC still has good robustness.

1 | INTRODUCTION

The bridge crane system is widely used as an important loading equipment in various industries, such as port transportation and equipment manufacturing [1, 2]. During the transportation of the bridge crane system, the inertia caused by the acceleration and the deceleration of the cart and the trolley, and the lifting action will cause the cargo to swing back and forth. This not only increases the possibility of accidents, but also seriously affects the improvement of production efficiency. Currently, the solution to this problem relies on the actual operating experience of the operator, which can realise the safe transportation and unloading of the cargo [2–5]. However, due to the long training period of the skilled technicians and the excessive work intensity, the working efficiency of the overall bridge travelling crane system is significantly restricted. Therefore, there is an urgent need for the automatic control system of the bridge crane system to solve the excessive dependence on operator experience [6–8]. The control of the bridge crane system includes many aspects, such as the positioning of the cart, the trajectory planning of the cart and the anti-sway control of the cargo [9, 10]. The anti-sway control of the cargo is the core

problem of the automatic control of the bridge crane system [11, 12]. Numerous methods, including the proportional–integral–derivative (PID) control method, have been proposed by scholars [13].

In recent years, numerous studies have been conducted on this issue. The traditional PID control method is relatively simple to implement and is currently the most widely used control method in practice. In [14–17], some improvements to traditional PID have been proposed. Soukkou et al. [14] and Ko [15] combined the fuzzy control with the PID control and designed a fuzzy-PID controller. Choi proposed a PID controller for the Lagrange system in [16]. Recently, Cuoghi and Ntogramatzidis [17] have proposed a new formula for the design of the PID controller for better steady-state performance and robustness. In [18], Ahmad et al. considered the model of double-pendulum-type overhead crane and proposed a single-input fuzzy control. In [19], Konstantopoulos and Alexandridis proposed open- and closed-loop control schemes and combined them together. Some scholars have applied a variety of intelligent control methods to control the bridge crane systems. A bridge crane system self-tuning controller based on a neural network is designed by Mendez et al. [20]. In

[21], Petrenko and Alavi presented a novel radial basis function neural network modelling method. Zhu and Wang [22] and Jahedi and Ardehali [23] combined the idea of genetic algorithm and fuzzy control and achieved good results. Many scholars used the sliding-mode control (SMC) method to conduct the research. SMC has a good effect on the tracking performance and also has good robustness. Wang et al. finished some modelling work and proposed two sliding-mode controller models [24]. Liu et al. [25] designed an adaptive sliding-mode fuzzy control approach. Sun et al. [26] constructed a sliding-mode-like strategy as well as an integral manifold. A second-order sliding-mode controller was proposed by Tuan et al. [27] for the control of a three-dimensional (3D) overhead crane with considering the uncertain system parameters. Moreover, for uncertain systems, an integral SMC method was proposed by Xi and Hesketh [28] for discrete-time systems. A recurrent fuzzy neural network SMC was designed by Lin and Shen [29], considering the model of the two-axis motion control system and adding robust control on the basis of fuzzy neural network.

SMC, also known as variable structure control, is essentially a nonlinear control strategy [30, 31]. The system is forced to follow a predetermined "sliding-mode" state trajectory. One advantage of SMC is that it is suitable for systems with uncertainties and, thus, has strong robustness with respect to disturbances and unmodelled dynamics. It is known that SMC usually provides good control performance for a general nonlinear system. However, traditional SMC approaches are not well designed for under-actuated systems, which may encounter difficulties in the sliding surface chattering elimination or suffer from slow responses. Noticing that a bridge crane system is featured to be under-actuated, a hierarchical global fast terminal sliding-mode control (H-GFTSMC) approach [32] is employed in this work to address the relevant control problems. The global fast terminal sliding-mode is chosen as the sub-sliding-mode surface, which ensures that the state reaches the sliding-mode surface in a relatively fast speed and then converges to an equilibrium point. The proposed method is able to control a bridge crane system for a wide range of cable length and additive disturbances. It results in better robustness compared with some existing methods, which facilitate its practical applications.

The arrangements of this study are as follows. The model of a bridge crane system is introduced in Section 2. In Section 3, a hierarchical global fast terminal sliding-mode controller is established that is suitable for the bridge crane system. In Section 4, the stability of the proposed controller is validated. Simulations are presented in Section 5. Some conclusions are drawn in Section 6.

2 | MODELLING OF A BRIDGE CRANE SYSTEM

2.1 | The main structure and characteristics of the bridge crane system

A bridge crane has three driving devices, i.e. the cart operation mechanism, the trolley operation mechanism and the lifting mechanism. The cart runs along the tracks laid on both elevated sides. Among them, the cart operating mechanism is responsible for moving the whole machine along the tracks overhead, the trolley moves the cargo on the bridge, while the lifting mechanism generates the vertical movement for the cargo.

In the bridge crane system, if only a cart or a trolley is in operation, the crane will have two-degree-of-freedom (2-DOF) movement, i.e. the displacement of the cart and the swing of the cargo, as shown in Figure 1(a). If the lifting mechanism also runs with the cart or the trolley, the bridge crane will have three DOFs, as shown in Figure 1(b). When the cart and the trolley operate simultaneously, the bridge crane and the cargo will move in 3D space, as shown in Figure 1(c). If the lifting mechanism is operated together with the cart and the trolley, the bridge crane system can have five DOFs, as shown in Figure 1(d).

In order to facilitate the modelling and simulation of the proposed controller, the following assumptions are made.

(i) Air resistance and wind effects are ignored.
(ii) The quality and the elasticity of the cable are ignored.
(iii) The friction at the connection between the wire cable and the trolley is ignored.
(iv) The nonlinearities of the transmission mechanism such as the trolley motor and the reducer are ignored. It is believed that the driving force of the trolley can be directly controlled by the output torque of the controller.
(v) The equilibrium point of the system is the stable.

2.2 | Dynamics modelling

The Lagrange equation is employed to describe the dynamic model of the bridge crane system. The general form of a Lagrange equation is

$$\frac{d}{dt}\left(\frac{\partial L}{\partial \dot{q}_i}\right) - \frac{\partial L}{\partial q_i} = Q_i (i = 1, 2, 3, 4, 5), \tag{1}$$

where q_i are generalised coordinates, $L = K_e - P$ is the Lagrange function, K_e is the Lagrangian kinetic energy of particle system, P is the potential energy of particles and Q_i is the generalised force of the particle system.

Consider that the main part of the dissipative force in the system is friction, which cannot be ignored. Therefore, a dissipative force term is added to the general form of the Lagrange equation [33]. Then, the Lagrange equation with a dissipative force term can be obtained as

$$\frac{d}{dt}\left(\frac{\partial L}{\partial \dot{q}_i}\right) - \frac{\partial L}{\partial q_i} + \frac{\partial T}{\partial \dot{q}_i} = Q_i (i = 1, 2, 3, 4, 5), \tag{2}$$

where T is the dissipative force function.

A 3D, four-DOF model has been selected as the research object, as shown in Figure 1(c), where M is the total mass

(a)

(b)

(c)

(d)
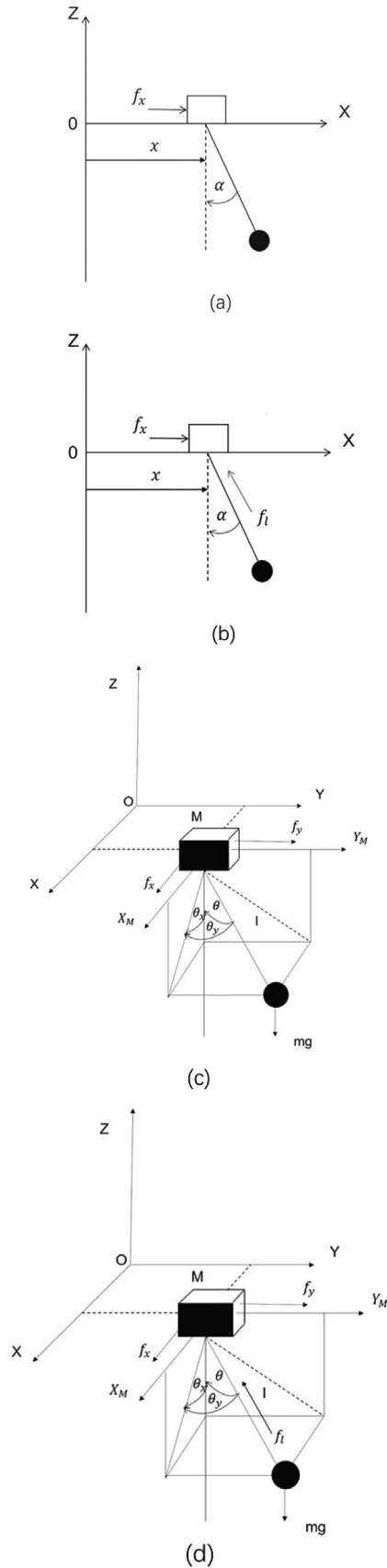
FIGURE 1   Bridge crane system model: (a) 2D, 2-DOF, (b) 2D, 3-DOF, (c) 3D, 4-DOF, and (d) 3D, 5-DOF

of the cart and the trolley, m is the mass of the cargo and its rotating system, l is the cable length, XYZ coordinate system is a fixed coordinate system with the initial position of the trolley as the origin and $X_M Y_M Z_M$ is a coordinate system with the cart's current position as the origin. The coordinate of the trolley on the XYZ coordinate system is $(x, y, 0)$; the coordinate system of the trolley is established, which is parallel to each axis of the cart coordinate system. Y_M is defined along the main beam, the direction of movement of the trolley is Y_M and the direction of movement of the main beam is X_M. θ is the angle between the cargo in any direction and the vertical direction. This angle has two components that can be decomposed into θ_x and θ_y. θ_x is the component of θ on the $X_M O Z_M$ plane; θ_y is the component of θ on the $Y_M O Z_M$ plane.

It is assumed that the coordinates of the cargo in the XYZ coordinate system are (x_m, y_m, z_m), which are given by

$$
\begin{aligned}
x_m &= x + l \sin \theta_x \cos \theta_y, \\
y_m &= y + l \sin \theta_y, \\
z_m &= -l \cos \theta_x \cos \theta_y,
\end{aligned}
\tag{3}
$$

where l is the cable length

Then, the following expressions are also given:

$$
\begin{aligned}
K_e &= \frac{1}{2}(M_x \dot{x}^2 + M_y \dot{y}^2 + M_l \dot{l}^2) + \frac{m}{2} v_m^2, \\
P &= mgl(1 - \cos \theta_x \cos \theta_y), \\
T &= \frac{1}{2}(D_x \dot{x}^2 + D_y \dot{y}^2 + D_l \dot{l}^2),
\end{aligned}
\tag{4}
$$

where K_e denotes the kinetic energy of the crane, P denotes the potential energy of the cargo and T denotes the dissipative force function. D_x, D_y and D_l denote the viscous damping coefficients associated with the x, y and l motions, respectively. v_m^2 is given as follows:

$$
\begin{aligned}
v_m^2 =& \dot{x}_m^2 + \dot{y}_m^2 + \dot{z}_m^2 \\
=& \dot{x}^2 + \dot{y}^2 + \dot{l}^2 + l^2 \cos^2 \theta_y \dot{\theta}_x^2 + l^2 \dot{\theta}_y^2 + 2(\sin \theta_y \dot{l} \\
& + l \cos \theta_y \dot{\theta}_y) \dot{y} + 2(\sin \theta_x \cos \theta_y \dot{l} + l \cos \theta_x \cos \theta_y \dot{\theta}_x \\
& - l \sin \theta_x \sin \theta_y \dot{\theta}_y) \dot{x}.
\end{aligned}
\tag{5}
$$

For the four-DOF bridge crane system model shown in Figure 1(c), the cable length will not change during the movement. Hence, it holds that $\dot{l} = \ddot{l} = 0$, which is then substituted into (3) and (4), resulting in the Lagrange function L and dissipative

force function T as follows:

$$L = K_e - P$$

$$= \frac{1}{2}(M_x \dot{x}^2 + M_y \dot{y}^2) + \frac{m}{2}v_m^2 \tag{6}$$

$$- mgl(1 - \cos\theta_x \cos\theta_y),$$

$$T = \frac{1}{2}(D_x \dot{x}^2 + D_y \dot{y}^2), \tag{}$$

where M_x and M_y are the x (travelling) and y (traversing) components of the total mass, which consists of the mass of the cart, the trolley and the equivalent mass of transmission mechanism; besides, m denotes the mass of cargo, g denotes the gravitational acceleration and v_m denotes the cargo speed.

Substituting (6) into (2), the dynamic equations of the four-DOF bridge crane system can be obtained as

$$(M_x + m)\ddot{x} + ml\cos\theta_x \cos\theta_y \ddot{\theta}_x - ml\sin\theta_x \sin\theta_y \ddot{\theta}_y$$

$$+ D_x \dot{x} - ml\sin\theta_x \cos\theta_y \dot{\theta}_x^2 - 2ml\cos\theta_x \sin\theta_y \dot{\theta}_x \dot{\theta}_y \tag{7}$$

$$- ml\sin\theta_x \cos\theta_y \dot{\theta}_y^2 = f_x,$$

$$(M_y + m)\ddot{y} + D_y \dot{y} + ml\cos\theta_y \ddot{\theta}_y - ml\sin\theta_y \dot{\theta}_y^2 = f_y, \tag{8}$$

$$ml^2\cos^2\theta_y \ddot{\theta}_x + ml\cos\theta_x \cos\theta_y \ddot{x} + mgl\sin\theta_x \cos\theta_y$$

$$- 2ml^2 \sin\theta_y \cos\theta_y \dot{\theta}_x \dot{\theta}_y = 0, \tag{9}$$

$$ml\cos\theta_y \ddot{y} - ml\sin\theta_x \sin\theta_y \ddot{x} + ml^2 \cos\theta_y \sin\theta_y \dot{\theta}_x^2$$

$$+ mgl\cos\theta_x \sin\theta_y + ml^2 \ddot{\theta}_y = 0, \tag{10}$$

where f_x and f_y are the driving forces of the motions in the x direction and the y direction.

Equations (7)–(10) can be written as the following matrix form:

$$M(q)\ddot{q} + D\dot{q} + C(q,\dot{q})\dot{q} + G(q) = F, \tag{11}$$

where

$$q = \begin{bmatrix} x & y & \theta_x & \theta_y \end{bmatrix}^T, \tag{12}$$

$$M(q) = \begin{bmatrix} M_{11} & M_{12} & M_{13} & M_{14} \\ M_{12} & M_{22} & M_{23} & M_{24} \\ M_{13} & M_{32} & M_{33} & M_{34} \\ M_{14} & M_{42} & M_{43} & M_{44} \end{bmatrix}, \tag{13}$$

$$C(q,\dot{q}) = \begin{bmatrix} 0 & 0 & C_{13} & C_{14} \\ 0 & 0 & C_{23} & C_{24} \\ 0 & 0 & C_{33} & C_{34} \\ 0 & 0 & C_{43} & C_{44} \end{bmatrix}, \tag{14}$$

$$D = \begin{bmatrix} D_x & 0 & 0 & 0 \\ 0 & D_y & 0 & 0 \\ 0 & 0 & 0 & 0 \\ 0 & 0 & 0 & 0 \end{bmatrix}, \tag{15}$$

$$G(q) = \begin{bmatrix} 0 \\ 0 \\ mgl\sin\theta_x \cos\theta_y \\ mgl\cos\theta_x \sin\theta_y \end{bmatrix}, \tag{16}$$

and

$$F = [f_x \ f_y]^T. \tag{17}$$

Readers may refer to the Appendix for details. Combining $C(q,\dot{q})$ and D into $\bar{C}(q,\dot{q})$, (11) can be simplified as follows:

$$M(q)\ddot{q} + \bar{C}(q,\dot{q})\dot{q} + G(q) = F, \tag{18}$$

where

$$\bar{C}(q,\dot{q}) = \begin{bmatrix} D_x & 0 & C_{13} & C_{14} \\ 0 & D_y & C_{23} & C_{24} \\ 0 & 0 & C_{33} & C_{34} \\ 0 & 0 & C_{43} & C_{44} \end{bmatrix}. \tag{19}$$

3 | DESIGN OF HIERARCHICAL GLOBAL FAST TERMINAL SLIDING-MODE CONTROLLER

The crane model given in (7)–(10) represents an under-actuated system. Generally speaking, the control of under-actuated systems is inconvenient compared with fully actuated ones. In this work, an H-GFTSMC method is used to address this problem. For under-actuated systems, the basic idea of the H-GFTSMC method is to divide the actuated and the under-actuated parts of the system into different sub-systems, and then design the lower layer sub-sliding surfaces and construct the total sliding surface of the upper layer surface, as shown in Figure 2. According to the sliding surfaces of the lower layer, the equivalent input in the sense of Filippov [34] is obtained, and the switching function is obtained using the feedback function [35] for the sliding surface of the upper layer. After the integration of the equivalent input terms and the switching control function term, the
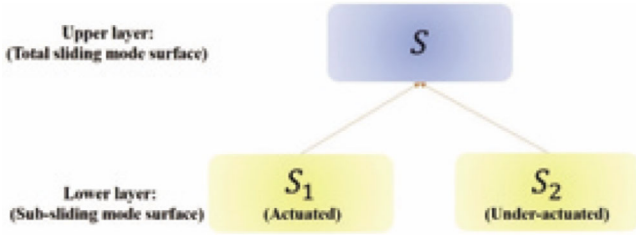
FIGURE 2 Schematic diagram of two-layer hierarchical SMC

total system input that can ensure the stability of the overall sliding surface can be obtained. The details are discussed in the following.

3.1 | Selection of target trajectory

In order to realise the stable control of the bridge crane system, a smooth s-shaped curve is used for the track of the vehicle. The target trajectory of the trolley investigated by Fang et al. [36] is employed in this work, i.e.

$$
\begin{aligned}
x_d =& \frac{P_{dx}}{2} + \frac{k_{vx}^2}{4k_{ax}} \ln(\cosh(2k_{ax}t/k_{vx} - \varepsilon_x) \\
& / \cosh(2k_{ax}t/k_{vx} - \varepsilon_x - 2P_{dx}k_{ax}/k_{vx}^2)), \\
y_d =& \frac{P_{dy}}{2} + \frac{k_{vy}^2}{4k_{ay}} \ln(\cosh(2k_{ay}t/k_{vy} - \varepsilon_y) \\
& / \cosh(2k_{ay}t/k_{vy} - \varepsilon_y - 2P_{dy}k_{ay}/k_{vy}^2)),
\end{aligned}
\tag{20}
$$

where t is the time and x_d and y_d are target trajectory of x and y directions, respectively; similarly, P_{dx} and P_{dy} are target positions of the vehicle, k_{vx} and k_{vy} are maximum speeds of the vehicle, k_{ax} and k_{ay} are maximum accelerations of the vehicle and ε_x and ε_y are initial acceleration parameters of the vehicle.

3.2 | Error dynamics

The target values of the swing angles θ_x and θ_y are set as 0. The desired system state is given as

$$
q_d = \begin{bmatrix} x_d\, y_d\, 0\, 0 \end{bmatrix}^T.
\tag{21}
$$

The dynamic equation for the errors is given by

$$
\begin{aligned}
& M(q)(\ddot{q} - \ddot{q}_d) + \bar{C}(q,\dot{q})(\dot{q} - \dot{q}_d) \\
& = F - G(q) - M(q)\ddot{q}_d - \bar{C}(q,\dot{q})\dot{q}_d.
\end{aligned}
\tag{22}
$$

Denote

$$
\begin{aligned}
e &= q - q_d, \\
&= \begin{bmatrix} x - x_d\, y - y_d\, \theta_x\, \theta_y \end{bmatrix}^T, \\
&= \begin{bmatrix} e_x\, e_y\, e_{\theta_x}\, e_{\theta_y} \end{bmatrix}^T,
\end{aligned}
\tag{23}
$$

$$
\begin{aligned}
U &= F - G(q) - M(q)\ddot{q}_d - \bar{C}(q,\dot{q})\dot{q}_d, \\
&= \begin{bmatrix} \sigma_x\, \sigma_y\, \sigma_{\theta_x}\, \sigma_{\theta_y} \end{bmatrix}^T,
\end{aligned}
\tag{24}
$$

where

$$
\begin{aligned}
\sigma_x &= f_x - (M_x + m)\ddot{x}_d - D_x\dot{x}_d, \\
\sigma_y &= f_y - (M_y + m)\ddot{y}_d - D_y\dot{y}_d, \\
\sigma_{\theta_x} &= -mgl\sin\theta_x\cos\theta_y - m\ddot{x}_dl\cos\theta_x\cos\theta_y, \\
\sigma_{\theta_y} &= -mgl\cos\theta_x\sin\theta_y + m\ddot{x}_dl\sin\theta_x\sin\theta_y \\
& \quad - m\ddot{y}_dl\cos\theta_y.
\end{aligned}
\tag{25}
$$

By using (23)–(25), (18) can be written as

$$
M(q)\ddot{e} + \bar{C}(q,\dot{q})\dot{e} = U.
\tag{26}
$$

3.3 | Hierarchical global fast terminal sliding-mode controller design

The error dynamics of the bridge crane system in (26) can be reformulated as

$$
\ddot{e} = M^{-1}(q)[U - \bar{C}(q,\dot{q})\dot{e}].
\tag{27}
$$

For convenience in analysis, two variables, viz. the displacement and the angle errors, are defined as

$$
e_p = \begin{bmatrix} e_x\, e_y \end{bmatrix}^T, \quad e_\theta = \begin{bmatrix} e_{\theta_x}\, e_{\theta_y} \end{bmatrix}^T.
\tag{28}
$$

The sliding surface of the lower layer is then designed for the displacement error of the vehicle and the swing angle error of the cargo

$$
S_1 = \dot{e}_p + H_1 e_p + \alpha \begin{bmatrix} e_x^{n/p} \\ e_y^{n/p} \end{bmatrix} = \begin{bmatrix} S_{1x} \\ S_{1y} \end{bmatrix}
$$

$$= \begin{bmatrix} \dot{e}_x + b_{1x}e_x + \alpha e_x^{n/p} \\ \dot{e}_y + b_{1y}e_y + \alpha e_y^{n/p} \end{bmatrix},$$

$$S_2 = \dot{e}_\theta + H_2 e_\theta + \beta \begin{bmatrix} e_{\theta_x}^{n/p} \\ e_{\theta_y}^{n/p} \end{bmatrix} = \begin{bmatrix} S_{2\theta_x} \\ S_{2\theta_y} \end{bmatrix}$$

$$= \begin{bmatrix} \dot{e}_{\theta_x} + b_{2\theta_x}e_{\theta_x} + \beta e_{\theta_x}^{n/p} \\ \dot{e}_{\theta_y} + b_{2\theta_y}e_{\theta_y} + \beta e_{\theta_y}^{n/p} \end{bmatrix}, \tag{29}$$

where $H_1 = \begin{bmatrix} b_{1x} & 0 \\ 0 & b_{1y} \end{bmatrix}$, $H_2 = \begin{bmatrix} b_{2\theta_x} & 0 \\ 0 & b_{2\theta_y} \end{bmatrix}$, and the parameters α, β, b_{1x}, b_{1y}, $b_{2\theta_x}$ and $b_{2\theta_y}$ are all positive constants; S_{1x}, S_{1y} and $S_{2\theta_x}$, $S_{2\theta_y}$ are the sub-sliding surfaces of the displacement and the swing angle in the x and y directions, respectively, and n and p are odd numbers satisfying $0 < n < p$.

The upper layer total sliding surface is defined as

$$S = I_1 S_1 + I_2 S_2 = \begin{bmatrix} S_x \\ S_y \end{bmatrix} = \begin{bmatrix} i_{1x}S_{1x} + i_{2\theta_x}S_{2\theta_x} \\ i_{1y}S_{1y} + i_{2\theta_y}S_{2\theta_y} \end{bmatrix}, \tag{30}$$

where $I_1 = \begin{bmatrix} i_{1x} & 0 \\ 0 & i_{1y} \end{bmatrix}$, $I_2 = \begin{bmatrix} i_{2\theta_x} & 0 \\ 0 & i_{2\theta_y} \end{bmatrix}$, and parameters i_{1x}, i_{1y}, $i_{2\theta_x}$ and $i_{2\theta_y}$ are all positive constants; S_x and S_y denote the components of S in the x and y directions, respectively.

According to the Filippov equivalence theory [37], one has

$$\dot{S}_1 = \ddot{e}_p + H_1 \dot{e}_p + \alpha(n/p) \begin{bmatrix} e_x^{n/p-1} & 0 \\ 0 & e_y^{n/p-1} \end{bmatrix} \dot{e}_p$$

$$= \ddot{e}_p + \bar{H}_1 \dot{e}_p = 0,$$

$$\dot{S}_2 = \ddot{e}_\theta + H_2 \dot{e}_\theta + \beta(n/p) \begin{bmatrix} e_{\theta_x}^{n/p-1} & 0 \\ 0 & e_{\theta_y}^{n/p-1} \end{bmatrix} \dot{e}_\theta$$ \tag{31}

$$= \ddot{e}_\theta + \bar{H}_2 \dot{e}_\theta = 0,$$

where $\bar{H}_1 = H_1 + \alpha(n/p) \begin{bmatrix} e_x^{n/p-1} & 0 \\ 0 & e_y^{n/p-1} \end{bmatrix}$, $\bar{H}_2 = H_2 + \beta(n/p) \begin{bmatrix} e_{\theta_x}^{n/p-1} & 0 \\ 0 & e_{\theta_y}^{n/p-1} \end{bmatrix}$.

For the convenience of the subsequent derivation process, (27) is changed into the following form:

$$\ddot{e}_p = A_1(e) + B_1(e)U = \begin{bmatrix} \ddot{e}_x \\ \ddot{e}_y \end{bmatrix} = \begin{bmatrix} A_{1x}(e) + B_{1x}(e)U \\ A_{1y}(e) + B_{1y}(e)U \end{bmatrix},$$ \tag{32}

$$\ddot{e}_\theta = A_2(e) + B_2(e)U = \begin{bmatrix} \ddot{e}_{\theta_x} \\ \ddot{e}_{\theta_y} \end{bmatrix} = \begin{bmatrix} A_{2x}(e) + B_{2x}(e)U \\ A_{2y}(e) + B_{2y}(e)U \end{bmatrix},$$

where $\begin{bmatrix} A_1(e) \\ A_2(e) \end{bmatrix} = [-M^{-1}(q)\bar{C}(q,\dot{q})\dot{e}]$, $\begin{bmatrix} B_1(e) \\ B_2(e) \end{bmatrix} = [M^{-1}(q)]$ and $A_1(e) = \begin{bmatrix} A_{1x}(e) \\ A_{1y}(e) \end{bmatrix}$, $A_2(e) = \begin{bmatrix} A_{2x}(e) \\ A_{2y}(e) \end{bmatrix}$ are matrices with the size 2×1, while $B_1(e) = \begin{bmatrix} B_{1x}(e) \\ B_{1y}(e) \end{bmatrix}$, $B_2(e) = \begin{bmatrix} B_{2x}(e) \\ B_{2y}(e) \end{bmatrix}$ are matrices with the size 2×4.

Substituting (32) into (31), the two equivalent outputs can be obtained

$$U_{eqp} = -B_1^{-1}(e)[\bar{H}_1 \dot{e}_p + A_1(e)],$$

$$U_{eq\theta} = -B_2^{-1}(e)[\bar{H}_2 \dot{e}_\theta + A_2(e)],$$ \tag{33}

where $B_1^{-1}(e)$ and $B_2^{-1}(e)$ are left pseudo-inverse matrices of $B_1(e)$ and $B_2(e)$, respectively, the dimensionalities of which are both 4×2.

For an under-actuated control system, it is necessary to make each sub-sliding surface stable in order to stabilised the closed-loop system. To this end, we consider the following control input:

$$\sigma_{total} = \sigma_1 + \sigma_2 + \sigma_{sw}, \tag{34}$$

where $\sigma_{total} = U$, $\sigma_1 = U_{eqp}$, $\sigma_2 = U_{eq\theta}$ and σ_{sw} is the switch term defined as

$$\sigma_{sw} = -(I_1 B_1(e) + I_2 B_2(e))^{-1}[I_2 B_2(e)\sigma_1 + I_1 B_1(e)\sigma_2 + WS + K\text{sgn}(S)],$$ \tag{35}

where $W = \begin{bmatrix} \omega_{3x} & 0 \\ 0 & \omega_{3y} \end{bmatrix}$, $K = \begin{bmatrix} k_{4x} & 0 \\ 0 & k_{4y} \end{bmatrix}$, and the parameters ω_{3x}, ω_{3y}, $k_{4\theta_x}$ and $k_{4\theta_y}$ are all positive constants.

Hence, one has

$$U = \sigma_{total} = \sigma_1 + \sigma_2 + \sigma_{sw}$$

$$= (I_1 B_1(e) + I_2 B_2(e))^{-1}[I_1 B_1(e)\sigma_1 + I_2 B_2(e)\sigma_2$$ \tag{36}

$$- WS - K\text{sgn}(S)],$$

which further results in the following inputs, as shown in (16):

$$f_x = \sigma_x + (M_x + m)\ddot{x}_d + D_x\dot{x}_d,$$

$$f_y = \sigma_y + (M_y + m)\ddot{y}_d + D_y\dot{y}_d.$$ \tag{37}

4 | STABILITY ANALYSIS

The stability of the hierarchical sliding-mode system can be proven only if all sliding surfaces are guaranteed to be stable. The stability analysis of the total sliding surface and sub-sliding surfaces is shown in this section.

4.1 | Stability of the total sliding surface

Theorem 1. *Consider the system (7)–(10) and the sliding-mode surfaces (29), (30) with the proposed H-GFTSMC law (36), S converges to 0 when t goes to infinity, that is* $\lim_{t\to\infty} S = 0$.

Proof. A positive-definite Lyapunov function is defined as $V = S^T S / 2$. Taking the time derivative of both sides of the Lyapunov function, one has

$$\dot{V} = S^T \dot{S}$$

$$= S^T (I_1 \dot{S}_1 + I_2 \dot{S}_2)$$

$$= S^T [I_1 (\ddot{e}_p + \bar{H}_1 \dot{e}_p) + I_2 (\ddot{e}_\theta + \bar{H}_2 \dot{e}_\theta)] \qquad (38)$$

$$= S^T [I_1 (A_1(e) + B_1(e)U + \bar{H}_1 \dot{e}_p)$$

$$+ I_2 (A_2(e) + B_2(e)U + \bar{H}_2 \dot{e}_\theta)].$$

Substituting (33) and (34) into (38), we obtain

$$\dot{V} = S^T [I_1 (\bar{H}_1 \dot{e}_p + A_1(e) - (\bar{H}_1 \dot{e}_p + A_1(e))$$

$$+ B_1(e)(\sigma_2 + \sigma_{\text{sw}})) + I_2 (\bar{H}_2 \dot{e}_\theta + A_2(e) \qquad (39)$$

$$- (\bar{H}_2 \dot{e}_\theta + A_2(e)) + B_2(e)(\sigma_1 + \sigma_{\text{sw}}))].$$

By substituting (35) into (39), it can be derived that

$$\dot{V} = S^T [-WS - K\text{sgn}(S)]$$

$$= -S^T WS - S^T K\text{sgn}(S) \leq 0. \qquad (40)$$

The equal sign holds if and only if $S = 0$. Since $V = \frac{1}{2} S^T S \geq 0$ and the inequality (40) is satisfied, the total sliding surface is asymptotic stable in the sense of Lyapunov, which guarantees that S converges to $\mathbf{0}$ as time goes to infinity. □

4.2 | Stability of the sub-sliding surfaces

The stability analysis of sub-sliding surfaces is given in the following. Note that S can be divided into two components, viz., S_x and S_y, which accounts for x and y directions, respectively. These two parts share similar kinematic structures and controller design strategies. The following Lyapunov functions are further proposed on this basis:

$$V_i = \frac{1}{2} S_i^2 (i \in \{x, y\}). \qquad (41)$$

In the following, the sliding surfaces in the x direction is mainly discussed.

From Section 4.1, we have known that $V_x = \frac{1}{2} S_x^2 \geq 0$, and $\dot{V}_x = -w_{3x} S_x^2 - k_{4x} |S_x| \leq 0$. Hence, we have

$$\int_0^t \dot{V}_x d\sigma = \int_0^t -\omega_{3x} S_x^2 - k_{4x} |S_x| d\sigma, \qquad (42)$$

which renders that

$$0 < V_x(t) = \frac{1}{2} S_x^2$$

$$= V_x(0) + \int_0^\infty -\omega_{3x} S_x^2 - k_{4x} |S_x| d\sigma \leq V_x(0) < \infty. \qquad (43)$$

Thus, $S_x \in L_\infty$, i.e. $\sup_{t \geq 0} |S_x| = ||S_x||_\infty < \infty$. Meanwhile, we have known that $\dot{V}_x = S_x \dot{S}_x = -w_{3x} S_x^2 - k_{4x} |S_x| < \infty$, so $\dot{S}_x \in L_\infty$, that is $\sup_{t \geq 0} |\dot{S}_x| = ||\dot{S}_x||_\infty < \infty$. Similarly, for the y direction, it holds $\sup_{t \geq 0} |S_y| = ||S_y||_\infty < \infty$ and $\sup_{t \geq 0} |\dot{S}_y| = ||\dot{S}_y||_\infty < \infty$.

Inequality (43) reveals that

$$\int_0^\infty \omega_{3x} S_x^2 + k_{4x} |S_x| d\sigma \leq V_x(0) < \infty. \qquad (44)$$

Since the sum of two positive terms is less than infinity in the above inequality, neither of the two terms goes to infinity. In other words, we have $\int_0^\infty |S_x| d\sigma < \infty$ and $\int_0^\infty S_x^2 d\sigma < \infty$, that is $S_x \in L_1$ and $S_x \in L_2$. Similarly, it holds $S_y \in L_1$ and $S_y \in L_2$.

Represent (32) as the following state-space model, which mainly involves variables corresponding to the x direction:

$$\begin{cases} \dot{x}_1 = x_2, \\ \dot{x}_2 = \ddot{e}_x = A_{1x}(e) + B_{1x}(e)U, \\ \dot{x}_3 = x_4, \\ \dot{x}_4 = \ddot{e}_{\theta_x} = A_{2x}(e) + B_{2x}(e)U. \end{cases} \qquad (45)$$

Note that for a practical crane system, the displacement and speed of the cart, the angle and angular velocity of the cargo, cannot be infinity. Hence, we proposed the following assumptions.

(i) All states are bounded, that is $||X||_\infty \leq \max(|x_1|, |x_2|, |x_3|, |x_4|) < \infty$.
(ii) $0 \leq \max(|A_{1x}(e)|, |A_{2x}(e)|) \leq \Lambda$, where Λ is a finite positive constant.
(iii) $B_{1x}(e)$ and $B_{2\theta_x}(e)$ are matrices determined by system parameters, whose elements are bounded. The matrix consisting of the maximum value of each item is B_M.
(iv) U is a matrix related to motor characteristics, whose elements are bounded. The matrix consisting of the maximum value of each item is U_M.

Theorem 2. *Consider the system (7)–(10) and the sliding-mode surfaces (29), (30) with the proposed H-GFTSMC law (36) and the above*

assumptions, S_{1x} and $S_{2\theta_x}$ converge to 0 when t goes to infinity, that is $\lim_{t \to \infty} S_{1x} = 0$, $\lim_{t \to \infty} S_{2\theta_x} = 0$.

Proof. From (29), it is known that

$$
\begin{aligned}
|S_{1x}| &= \left| \dot{e}_x + b_{1x} e_x + \alpha e_x^{n/p} \right| \\
&\leq |\dot{e}_x| + |b_{1x} e_x| + \left| \alpha e_x^{n/p} \right| \\
&\leq \|X\|_\infty + b_{1x} \|X\|_\infty + \alpha \|X\|_\infty^{n/p} < \infty.
\end{aligned}
\tag{46}
$$

Similarly, it can be derived that $|S_{2\theta_x}| < \infty$. Hence, $S_{1x} \in L_\infty$ and $S_{2\theta_x} \in L_\infty$.

From (31), one has

$$
\begin{aligned}
|\dot{S}_{1x}| &= \left| \ddot{e}_x + b_{1x} \dot{e}_x + \alpha(n/p) e_x^{n/p-1} \cdot \dot{e}_x \right| \\
&= \left| b_{1x} \dot{e}_x + \alpha(n/p) e_x^{n/p-1} \cdot \dot{e}_x + A_{1x}(e) + B_{1x}(e)U \right| \\
&\leq |b_{1x} \dot{e}_x| + \left| \alpha(n/p) e_x^{n/p-1} \right| |\dot{e}_x| + |A_{1x}(e)| + |B_{1x}(e)U| \\
&\leq b_{1x} \|X\|_\infty + \alpha(n/p)\|X\|_\infty^{n/p} + \Lambda + B_M \cdot U_M < \infty.
\end{aligned}
\tag{47}
$$

Similarly, it holds $|\dot{S}_{2\theta_x}| < \infty$. Thus, $\dot{S}_{1x} \in L_\infty$ and $\dot{S}_{2\theta_x} \in L_\infty$.

During the deriving process of H-GFTSMC, the value of i_{1x} does not affect the stability of the system. A new sliding surface $\hat{S}_x$ is introduced as

$$
\hat{S}_x = \hat{i}_{1x} S_{1x} + i_{2\theta_x} S_{2\theta_x},
\tag{48}
$$

where $\hat{i}_{1x}$ is a positive constant and $\hat{i}_{1x} \neq i_{1x}$. So $\hat{S}_x \neq S_x$. We also assume that $0 < \int_0^\infty \hat{S}_x^2 d\sigma \leq \int_0^\infty S_x^2 d\sigma < \infty$.

It is easy to derive that

$$
0 < \int_0^\infty S_x^2 - \hat{S}_x^2 d\sigma
$$

$$
= \int_0^\infty (i_{1x}^2 - \hat{i}_{1x}^2) S_{1x}^2 + 2(i_{1x} - \hat{i}_{1x}) S_{1x} i_{2\theta_x} S_{2\theta_x} d\sigma < \infty.
\tag{49}
$$

Substituting (30) into the above inequality, one has

$$
\int_0^\infty S_x^2 - \hat{S}_x^2 d\sigma
$$

$$
= \int_0^\infty (i_{1x}^2 - \hat{i}_{1x}^2) S_{1x}^2 + 2(i_{1x} - \hat{i}_{1x}) S_{1x}(S_x - i_{1x} S_{1x}) d\sigma
$$

$$
= \int_0^\infty -(i_{1x} - \hat{i}_{1x})^2 S_{1x}^2 d\sigma + \int_0^\infty 2(i_{1x} - \hat{i}_{1x}) S_{1x} S_x d\sigma > 0,
\tag{50}
$$

which implies that

$$
\begin{aligned}
\int_0^\infty (i_{1x} - \hat{i}_{1x})^2 S_{1x}^2 d\sigma &< \int_0^\infty 2(i_{1x} - \hat{i}_{1x}) S_{1x} S_x d\sigma \\
&\leq \int_0^\infty |2(i_{1x} - \hat{i}_{1x}) S_{1x} S_x| d\sigma \\
&\leq 2|(i_{1x} - \hat{i}_{1x})| \int_0^\infty \|S_{1x}\|_\infty |S_x| d\sigma \\
&\leq 2|(i_{1x} - \hat{i}_{1x})| \cdot \|S_{1x}\|_\infty \cdot \|S_x\|_1 < \infty.
\end{aligned}
\tag{51}
$$

Hence, it holds $S_{1x} \in L_2$. In a similar way, it can be derived that $S_{2\theta_x} \in L_2$. At this point, we have proved that $S_{1x} \in L_\infty$, $S_{2\theta_x} \in L_\infty$, $\dot{S}_{1x} \in L_\infty$, $\dot{S}_{2\theta_x} \in L_\infty$ and $S_{1x} \in L_2$, $S_{2\theta_x} \in L_2$; according to Barbalat's lemma [38], it holds that $\lim_{t \to \infty} S_{1x} = 0$ and $\lim_{t \to \infty} S_{2\theta_x} = 0$. The proof is thus complete. □

In a similar way, one can derive that $S_{1y} \in L_\infty$, $S_{2\theta_y} \in L_\infty$, $\dot{S}_{1y} \in L_\infty$, $\dot{S}_{2\theta_y} \in L_\infty$ and $S_{1y} \in L_2$, $S_{2\theta_y} \in L_2$, which render $\lim_{t \to \infty} S_{1y} = 0$ and $\lim_{t \to \infty} S_{2\theta_y} = 0$.

According to [39], the reaching time of the sub-sliding surfaces is given by the following equations:

$$
\begin{aligned}
t_{s_i} &= \frac{n}{b_{1i}(n-p)} \ln \frac{b_{1i} e_i(0)^{(n-p)/n} + \alpha}{\alpha}, \\
t_{s_{\theta_i}} &= \frac{n}{b_{2\theta_i}(n-p)} \ln \frac{b_{2\theta_i} e_{\theta_i}(0)^{(n-p)/n} + \beta}{\beta},
\end{aligned}
\tag{52}
$$

where $i \in \{x, y\}$, and t_{s_i} and $t_{s_{\theta_i}}$ are the reaching time of the displacement sliding surface and the swing angle sliding surface, respectively ($\max\{t_{s_i}, t_{s_{\theta_i}}\} \leq t_s$).

In summary, this section proves the asymptotic stability of all sliding surfaces of the system and shows that the controller can drive the system to the sliding surface in finite time and finally stabilise at the target position.

Remark 1. Generally speaking, the adjustment methods of sliding-mode parameters are mostly trial and error [40–42]. For the hierarchical sliding-mode system, the parameters of the lower sliding functions are generally considered first. After adjusting the parameters of the lower sliding functions, the upper sliding-mode parameters are adjusted, while the lower sliding-mode parameters are fine-tuned [43]. Although the considered system in (7)–(10) is an ideal system, the value of K still has a certain degree of robustness. If the upper and lower bounds of the disturbance are known, we can use the method mentioned in [44] to solve the range of K.

Remark 2. The proposed approach can be further improved by considering some latest research achievements. For example, extend the result to stochastic systems, as shown in [45]. When limited communication resources are available, one could consider event-triggered strategy in the design [46, 47], in which cases the system state may be updated only when it is necessary.

5 | SIMULATIONS

Several simulations have been undertaken to verify the control effect of the proposed controller. Simulation 1 shows the control performance of the proposed controller, and it is compared with PID in simulation 2. In simulation 3, the cable length was changed to demonstrate the robustness of the control method. In simulation 4, white noise was added to the proposed controller and compared with PID as well. The controller parameters used in the simulations are selected as

$$H_1 = \begin{bmatrix} 0.8 & 0 \\ 0 & 0.8 \end{bmatrix}, H_2 = \begin{bmatrix} 0.4 & 0 \\ 0 & 0.016 \end{bmatrix},$$

$$I_1 = \begin{bmatrix} 9 & 0 \\ 0 & 84 \end{bmatrix}, I_2 = \begin{bmatrix} 12 & 0 \\ 0 & 110 \end{bmatrix}, \tag{53}$$

$$W = \begin{bmatrix} 10 & 0 \\ 0 & 50 \end{bmatrix}, K = \begin{bmatrix} 0.03 & 0 \\ 0 & 0.028 \end{bmatrix}.$$

The related parameters are given by $g = 9.81$ m/s^2, $m = 30$ kg, $M_x = 1440$ kg, $M_y = 110$ kg, $D_x = 480$ kg/s, $D_y = 40$ kg/s, $P_{dx} = 50$ m, $P_{dy} = 20$ m, $k_{ax} = 0.25$ m/s^2, $k_{ay} = 0.08$ m/s^2, $k_{vx} = 1.05$ m/s, $k_{vy} = 0.53$ m/s, $\varepsilon_x = \varepsilon_y = 2.5$, $l = 10$ m, $\alpha = 1$, $\beta = 0.5$, $n = 1$, $p = 5$. In the simulations, the initial system state is $(x_0, y_0, \theta_{x0}, \theta_{y0}) = (0, 0, 0, 0)$, while the target state is set as $(x_d, y_d, \theta_{xd}, \theta_{yd}) = (50, 20, 0, 0)$.

5.1 | Control performance of H-GFTSMC

The simulation results are discussed in the following. The track of the trolley and the swing angle diagram of the cargo is illustrated in Figure 3. It can be seen in Figure 3(a) and (c) that the displacement trajectory of the vehicle is basically consistent with the target trajectory. It can also been in Figure 3(b) that the swing angle of the cargo has almost no swing outside the start and stop time. When the crane starts, the angle of the pendulum in the x direction reaches its maximum value of -0.06 rad in about 5 s. Meanwhile, the angle of the pendulum in the y direction reaches the maximum value of -0.018 rad in about 9 s. When the crane stops, the angles in x and y directions reach the maximum value of 0.058 and 0.019 rad in about 54 and 48 s, respectively. Outside these two time periods, the angle decays rapidly to zero. Under the control of H-GFTSMC, the displacement tracking of the trolley is good, and the pendulum angles in both x and y directions are limited to a small range. The driving force is demonstrated in Figure 3(d), which reveals that high-frequency chattering occurs during the starting and stopping periods. It is worth mentioning that reducing the value of k_{4x} and k_{4y} can mitigate this phenomenon, but is not able to eliminate it.

All the sliding surfaces of the entire system are shown in Figure 4, where Figure 4(a) and (b) shows the displacement dependent sub-sliding surface and the pendulum-angle-dependent sub-sliding surface, respectively. During the process of starting and stopping of the bridge crane system, each sub-sliding surface will fluctuate, but it will converge to 0 soon. It can be seen from Figure 4(a) and (b) that the two sub-sliding surfaces enter the sliding-mode movement soon after the simulation starts and then stabilise near the designed sliding surface. It can be seen from Figure 4(c) that the total sliding surface of the system is stable near 0 except for the start and stop phases. Hence, the simulation results show the effectiveness of the designed hierarchical global fast terminal sliding-mode controller.

5.2 | Performance comparison with a PID controller

So as to show the superiority of the proposed control method, its control performance is compared with the traditional PID control method, and the simulation results are as follows.

Because of the controller design process of the vehicle in x and y directions is the same, the motion in the x direction is analysed separately with PID.

Figure 5 shows the comparison of control performance of cart under H-GFTSMC and PID controllers. It can be seen from Figure 5(a) that the performance of trajectory tracking under the H-GFTSMC is excellent. The cart basically runs along the planned trajectory, and there is almost no overshooting when it stops. However, under the traditional PID control, the responding speed of cart is slow, and certain overshoot occurs when stopping. In Figure 5(b), the cargo swings slightly at start and stop, and returns to 0 rapidly in the rest of the time. In contrast, the pendulum angle under the PID control is slightly lower than that under the H-GFTSMC control, but there is always a certain pendulum angle during the operation process. Therefore, the H-GFTSMC method has obvious advantages compared with the traditional PID control method.

5.3 | Robustness with respect to cable lengths and additive white noises

Next, the controller robustness is simulated and analysed. The robustness is verified by changing the length of the hanging cable. Figures 6 and 7 show the simulation results of increasing and decreasing the length of hoisting cable, respectively.

The cable length of the controller is set to 10 m; on the other side, the actual cable length is set to be 5 and 15 m.

Comparing Figures 3(a) and 6(a) shows that the curve fluctuation in Figure 6(a) does not increase significantly. Even if the cable length is shortened, the controller can still obtain a better displacement tracking performance. From Figures 3(b) and 6(b), there is no significant swing amplitude change in the swing angle of the cargo, and the anti-swing control performance is still good. Therefore, when the cable length is shortened, the control performance of the controller is still considerable.

When the cable length is increased, the displacement tracking performance is good, with no large tracking error, as shown in Figures 3(a) and 7(a). However, there are some problems with
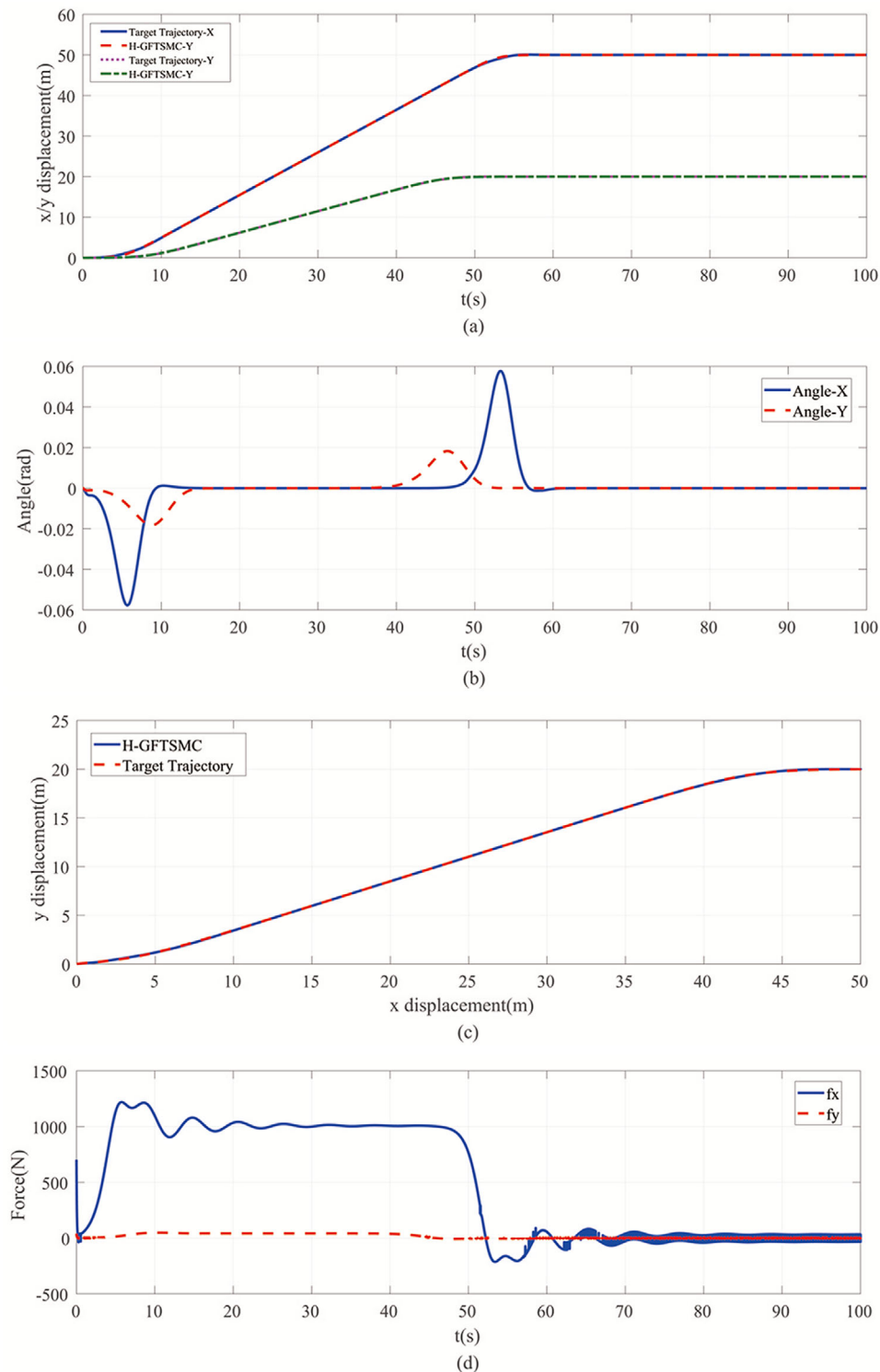
FIGURE 3 Control performance of the proposed method. (a) The trolley trajectory and its reference signal. (b) The angular of the cargo suspended in the x and y directions. (c) Top view of the vehicle spatial displacement. (d) Driving forces in x and y directions

the angle. As shown in Figure 7(b), when the crane starts and stops, the pendulum angle has some small fluctuations and is unable to return to 0 quickly.

All above simulations are conducted under the ideal conditions. Due to issues such as sensor accuracy, there must be a lot

of noise that cannot be ignored. Therefore, on the basis of simulations 1 and 2, Gaussian white noise is added to the feedback collected by the system to verify the robustness of the proposed control method in the presence of interference. The simulation results are shown in Figure 8.
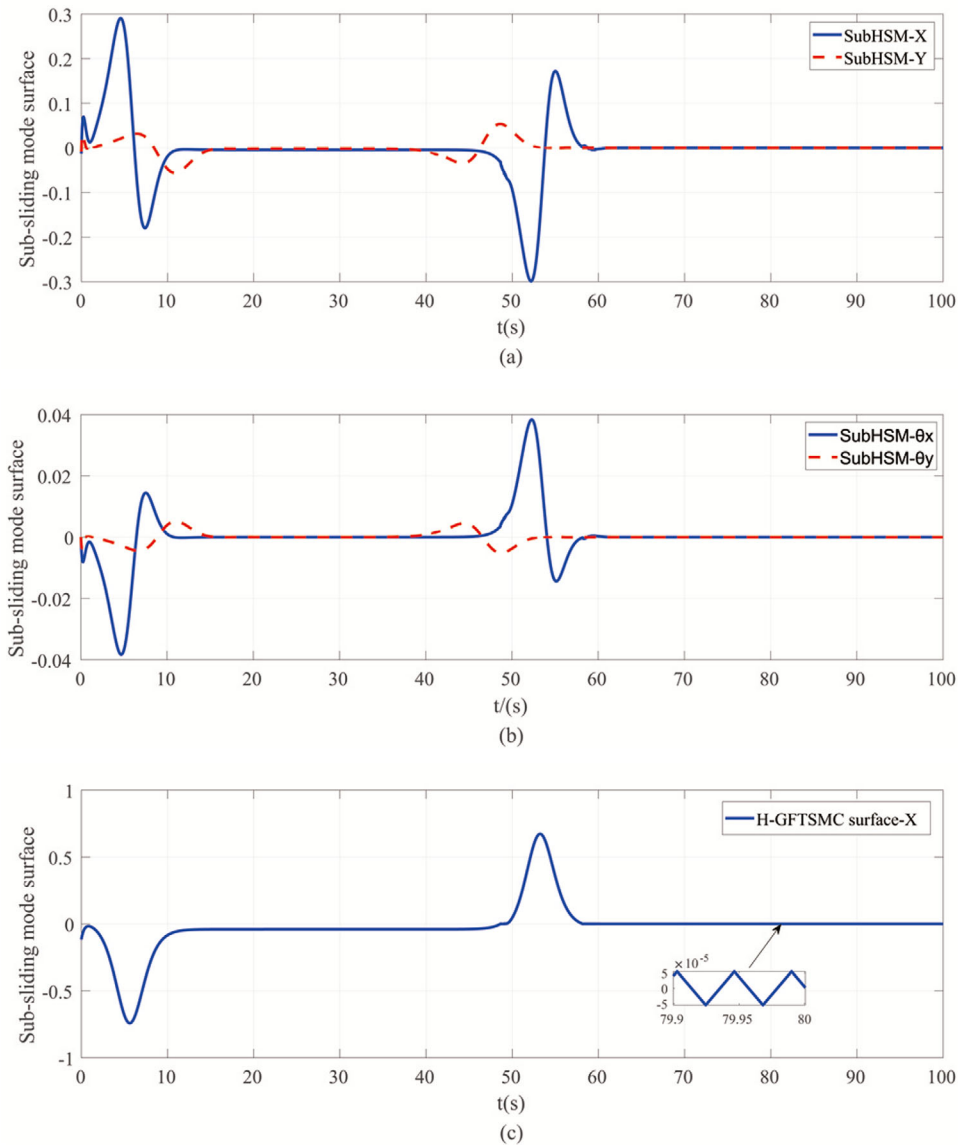
FIGURE 4 All sliding-mode surfaces. (a) The sub-sliding surface of the displacement-dependent sub-system. (b) Sub-sliding surface of the sub-system related to the pendulum angle. (c) Total sliding surface of the whole system

It can be seen from Figure 8(a) that the trajectory of the cart and the ideal trajectory almost coincide. We further compare the proposed H-GFTSMC with the PID control strategy presented in Section 5.2. White noise is added to the system to verify the robustness of various control methods. As shown in Figure 7, the swing angle amplitude using H-GFTSMC is relatively small. Besides, the proposed approach outperforms the PID controller with respect to the trajectory tracking. H-GFTSMC renders small oscillations around the target trajectory, while the PID controller leads to a large deviation.

6 | CONCLUSION

This paper proposes an H-GFTSMC to handle the problem of large cargo swing during the operation of the bridge crane system. First, the Lagrangian dynamic modelling of the bridge crane system is conducted. Then, the hierarchical global fast terminal sliding-mode controller is designed according to the under-actuated characteristics of the system. The stability of the proposed controller is verified, and it is proved that all sliding surfaces of the controller can reach the stable state in a limited time. Finally, the simulation results demonstrate that the controller has better restraining performance on the swing angle of the cargo compared with PID, and the controller still has good robustness when the cable length is changed. Moreover, the performance of the controller is still excellent even when the feedback signal contains noise. In our future work, we will improve the proposed H-GFTSMC strategy by considering event-trigging mechanisms, which can be employed for applications with limited communication resources.
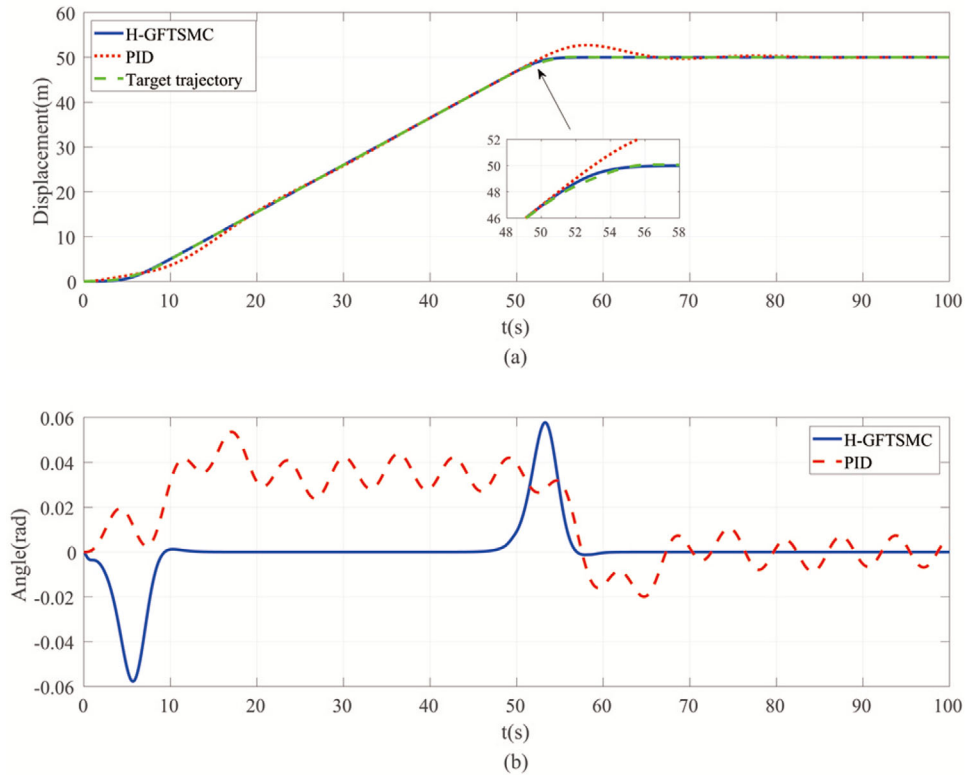
FIGURE 5   (a) Comparison of the displacement. (b) Comparison of the angles
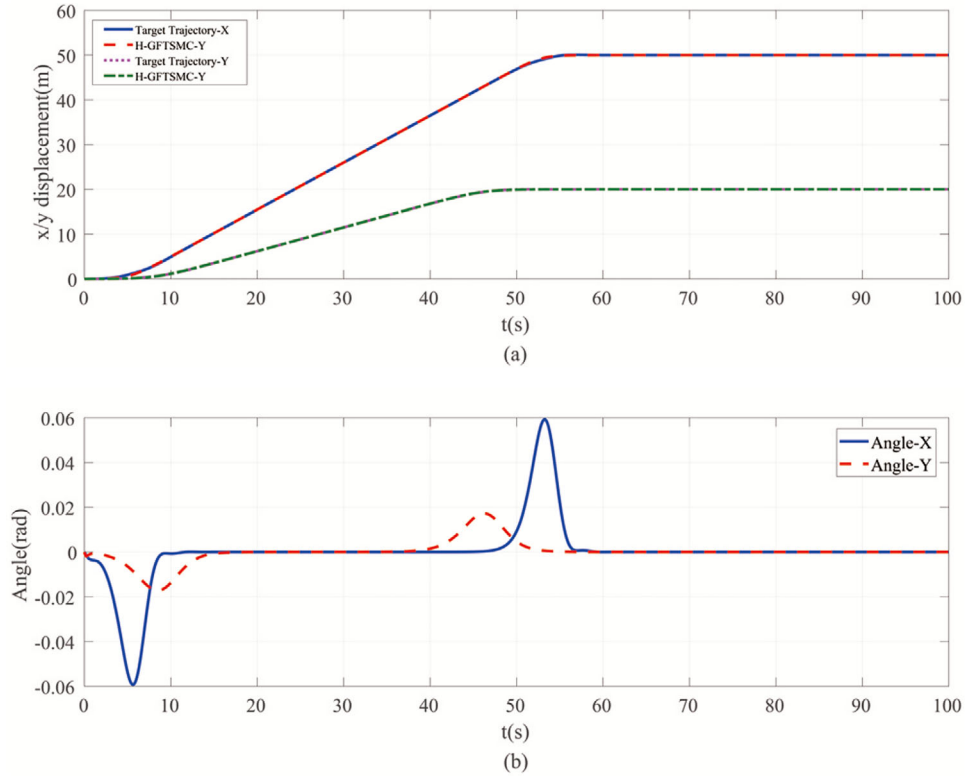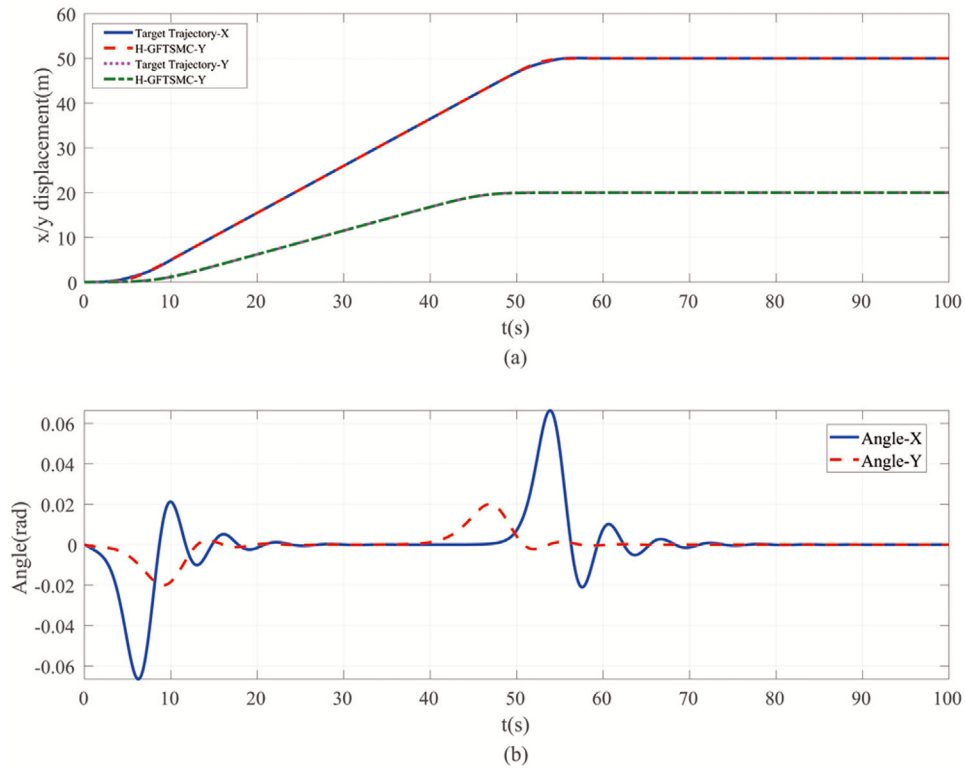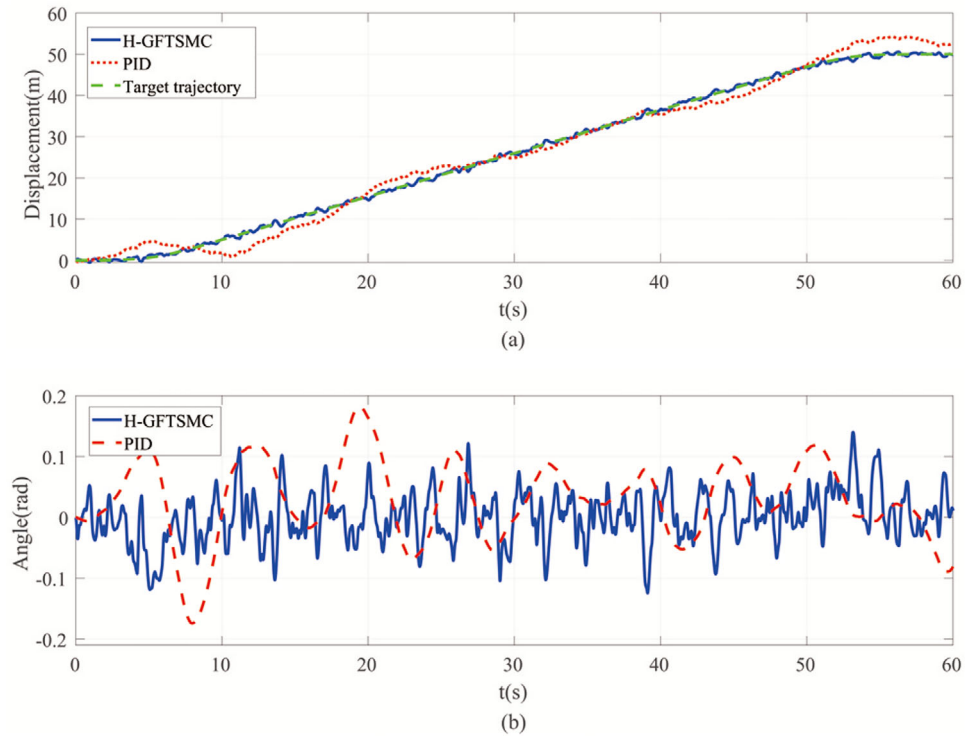

FIGURE 6   The performance of shortening the length of hanging cable on the (a) displacement and (b) angles

FIGURE 7 The performance of increasing the length of hanging cable on the (a) displacement and (b) angles

FIGURE 8 The comparisons between H-GFTSMC and PID on adding white noise: (a) displacement and (b) angles

ACKNOWLEDGEMENT

DATA AVAILABILITY STATEMENT

The data that support the findings of this study are available from the corresponding author upon reasonable request.

CONFLICT OF INTEREST STATEMENT

We declare that we have no financial and personal relationships with other people or organisations that can inappropriately influence our work; there is no professional or other personal interest of any nature or kind in any product, service and/or company that could be construed as influencing the position presented in, or the review of, the manuscript entitled.

PERMISSION STATEMENT

Permission statement for reproducing the materials like trademark image and copyrights image in the manuscript: None.

ORCID

Weilin Yang https://orcid.org/0000-0003-3112-3372

REFERENCES

1. Novel, B., Coron, J.M.: Exponential stabilization of an overhead crane with flexible cable via a back-stepping approach. Automatica 36 (4), 587–593 (2000)
2. Manson, G.A.: Time-optimal control of an overhead crane model. Optimal Control Appl. Methods. 3 (2), 115–120 (1982)
3. Mansour, A., Karkoub, M.A.K.: Robust control schemes for an overhead crane, J. Vib. Control 7(3), 395–416 (2001)
4. Nourollahi, et al.: Full shift assessment of back and head postures in overhead crane operators with and without symptoms. J Occup. Health 60 (1), 46–54 (2018)
5. Zhao, Y., Gao, H.: Fuzzy-model-based control of an overhead crane with input delay and actuator saturation. IEEE Trans. Fuzzy Syst. 20 (1), 181–186 (2012)
6. Srivastava, N.K., Mondal, S.: Development of predictive maintenance model of an overhead crane exercising NHPP models. IJCSMS Int. J. Comput. Sci. Manage. Stud. 13 (3), 71–77 (2013)
7. Moustafa, K.A.F., Ebeid, A.M.: Nonlinear modeling and control of overhead crane load sway. J. Dyn. Syst. Meas. Control 110 (3), 266–271 (1988)
8. Lee, H.H.: Modeling and control of a three-dimensional overhead crane. J. Dyn. Syst. Meas. Control 120 (4), 471–476 (1998)
9. Liu, R., Li, S., Ding, S.: Nested saturation control for overhead crane systems. Trans. Inst. Meas. Control 34 (7), 862–875 (2012)
10. Nguyen, H.T.: State-variable feedback controller for an overhead crane. J. Electr. Electron. Eng. 14 (2), 75–84 (1994)
11. Mahfouf, M. et al.: Fuzzy logic-based anti-sway control design for overhead cranes. Neural Comput. Appl. 9 (1), 38–43 (2000)
12. Yoshida, Y., Tabata, H.: Visual feedback control of an overhead crane and its combination with time-optimal control. In: IEEE/ASME International Conference on Advanced Intelligent Mechatronics, pp. 1114–1119 (2008)
13. Yang, J.H., Shen, S.H.: A novel approach for the adaptive tracking control for 3-D overhead crane system. In: International Conference on Modelling, pp. 446–450. Shanghai, China (2008)
14. Soukkou, A., Khellaf, A., Leulmi, S.: Control of overhead crane by fuzzy-PID with genetic optimisation. In: IFIP International Federation for Information Processing, pp. 67–80. Springer, Boston, MA (2004)
15. Ko, C.N.: A fuzzy PID controller based on hybrid optimization approach for an overhead crane. In: Communications in Computer and Information Science, pp. 202–209. Springer, Berlin, Germany (2011)
16. Choi, Y.: PID state estimator for Lagrangian systems. IET Control Theory Appl. 1 (4), 937–945 (2007)
17. Cuoghi, S., Ntogramatzidis, L.: Direct and exact methods for the synthesis of discrete-time proportional-integral-derivative controllers. IET Control Theory Appl. 7 (18), 2164–2171 (2013)
18. Ahmad, M.A. et al.: Single input fuzzy controller with command shaping schemes for double-pendulum-type overhead crane. AIP Conf. Proc. 1337(1), 1397–1402 (2011)
19. Konstantopoulos, G.C., Alexandridis, A.T: Simple energy based controllers with nonlinear coupled-dissipation terms for overhead crane systems. In: IEEE Conference on Decision and Control, pp. 3149–3154 (2009)
20. Mendez, J.A. et al.: Design of a neural network based self-tuning controller for an overhead crane. In: IEEE International Conference on Control Applications, pp. 168–171. Trieste, Italy (1998)
21. Petrenko, Y.N., Alavi, S.E.: Fuzzy logic and genetic algorithm technique for non-liner system of overhead crane. In: IEEE Region 8 International Conference on Computational Technologies in Electrical and Electronics Engineering, pp. 848–851. IEEE, Listvyanka, Russia (2010)
22. Zhu, X., Wang, N.: Cuckoo search algorithm with membrane communication mechanism for modeling overhead crane systems using RBF neural networks. Appl. Soft Comput. 56, 458–471 (2017)
23. Jahedi, G., Ardehali, M.M.: Genetic algorithm-based fuzzy-PID control methodologies for enhancement of energy efficiency of a dynamic energy system. Energy Convers. Manage. 52 (1), 725–732 (2011)
24. Wang, W., et al.: Structure design of two types of sliding-mode controllers for a class of under-actuated mechanical systems. IET Control Theory Appl. 1 (1), 163–172 (2007)
25. Liu, D. et al.: Adaptive sliding mode fuzzy control for a two-dimensional overhead crane. Mechatronics 15 (5), 505–522 (2005)
26. Sun, N., et al.: A new antiswing control method for underactuated cranes with unmodeled uncertainties: Theoretical design and hardware experiments. IEEE Trans. Ind. Electron. 62 (1), 453–465 (2015)
27. Tuan, L.A. et al.: Second-order sliding mode control of a 3D overhead crane with uncertain system parameters. Int. J. Precis. Eng. Manuf. 15 (5), 811–819 (2014)
28. Xi, Z., Hesketh, T.: Discrete time integral sliding mode control for overhead crane with uncertainties. IET Control Theory Appl. 4 (10), 2071–2081 (2010)
29. Lin, F.-J., Shen, P.-H.: Robust fuzzy neural network sliding-mode control for two-axis motion control system. IEEE Trans. Ind. Electron. 53 (4), 1209–1225 (2006)
30. Bartolini, G. et al.: A survey of applications of second-order sliding mode control to mechanical systems. Int. J. Control 76 (9-10), 875–892 (2003)
31. Bandyopadhyay, B., et al.: Integral sliding mode based composite nonlinear feedback control. In: Sliding Mode Control Using Novel Sliding Surfaces, pp. 83–95. Springer, Berlin, Germany (2009)
32. Wang, W. et al.: Design of a stable sliding-mode controller for a class of second-order underactuated systems. IEE Proc.—Control Theory Appl. 151 (6), 683–690 (2004)
33. Close, C.M., Frederick, D.K.: Modeling and Analysis of Dynamic Systems. Taylor & Francis, New York (2014)
34. Filippov, A.F.: Differential equations with discontinuous righthand sides. J. Math. Anal. Appl. 154 (2), 99–128 (1999)
35. Nai, et al.: Discrete output feedback sliding-mode control with integral action. Int. J. Robust Nonlinear Control 216 (1), 21–43 (2006)
36. Fang, Y., et al.: A motion planning-based adaptive control method for an underactuated crane system, IEEE Trans. Control Syst. Technol. 20(1), 241–248 (2011)
37. Filippov, A.G.: Application of the theory of differential equations with discontinuous right-hand sides to non-linear problems in automatic control. IFAC Proc. Vol. 1 (1), 933–937 (1960)
38. Tao, G.: A simple alternative to the Barbalat lemma. IEEE Trans. Autom. Control 42 (5), 698 (2002)

39. Min, J., Fang, Y., Xu, Z.: Adaptive fast terminal sliding mode control for a class of uncertain system. In: International Conference on Industrial and Information Systems, pp. 337–340 (2009)
40. Bartolini, G., et al.: Chattering avoidance by second-order sliding mode control. IEEE Trans. Autom. Control 43 (2), 241–246 (2002)
41. Feng, Y., Yu, X., Man, Z.: Non-singular terminal sliding mode control of rigid manipulators. Automatica 38 (12), 2159–2167 (2002)
42. Utkin, V.I., Chang, H-C.: Sliding mode control on electro-mechanical systems. Math. Prob. Eng. 8 (4-5), 451–473 (2002)
43. Wang, J-J., Liu, G-Y.: Hierarchical sliding-mode control of spatial inverted pendulum with heterogeneous comprehensive learning particle swarm optimization. Inf. Sci. 495, 14–36 (2019)
44. Li, J., Niu, Y.: Sliding mode control subject to rice channel fading. IET Control Theory Appl. 12 (16), 2529–2537 (2019)
45. Song, J. et al.: Asynchronous sliding mode control of singularly perturbed semi-Markovian jump systems: application to an operational amplifier circuit. Automatica 118, 109026 (2020)
46. Yang, Y., Niu, Y.: Event-triggered adaptive neural backstepping control for nonstrict-feedback nonlinear time-delay systems. J. Franklin Inst. 357 (8), 4624–4644 (2020)
47. Song, J., Ho, D.W.C., Niu, Y.: Model-based event-triggered sliding-mode control for multi-input systems: Performance analysis and optimization. IEEE Trans. Cybern. to be published. https://doi.org/10.1109/TCYB.2020.3020253

APPENDIX
The Parameters in (12)

$$M_{11} = M_x + m \qquad M_{12} = 0$$
$$M_{13} = ml \cos\theta_x \cos\theta_y \qquad M_{14} = -ml \sin\theta_x \sin\theta_y$$
$$M_{21} = 0 \qquad M_{22} = M_y + m$$
$$M_{23} = 0 \qquad M_{24} = ml \cos\theta_y$$
$$M_{31} = ml \cos\theta_x \cos\theta_y \qquad M_{32} = 0$$
$$M_{33} = ml^2 \cos^2\theta_y \qquad M_{34} = 0$$
$$M_{41} = -ml \sin\theta_x \sin\theta_y \qquad M_{42} = ml \cos\theta_y$$
$$M_{43} = 0 \qquad M_{44} = ml^2$$

$$C_{13} = -ml \sin\theta_x \cos\theta_y \dot\theta_x - ml \cos\theta_x \sin\theta_y \dot\theta_y$$
$$C_{14} = -ml \cos\theta_x \sin\theta_y \dot\theta_x - ml \sin\theta_x \cos\theta_y \dot\theta_y$$
$$C_{23} = 0$$
$$C_{24} = -ml \sin\theta_y \dot\theta_y$$
$$C_{33} = -ml^2 \sin\theta_y \cos\theta_y \dot\theta_y$$
$$C_{34} = -ml^2 \sin\theta_y \cos\theta_y \dot\theta_x$$
$$C_{43} = ml^2 \cos\theta_y \sin\theta_y \dot\theta_x$$
$$C_{44} = 0.$$